Title

Spectral Graph modeling of abnormal neural synchronizations in Alzheimer's disease

ISBN

9798189293955

Author

Debnath, Apurba

Publication Date

2026-09-03

Peer reviewed|Thesis/dissertation

Spectral Graph modeling of abnormal neural synchronizations in Alzheimer's disease

by
Apurba Debnath

THESIS
Submitted in partial satisfaction of the requirements for degree of
MASTER OF SCIENCE

in

Biomedical Imaging

in the

GRADUATE DIVISION
of the
UNIVERSITY OF CALIFORNIA, SAN FRANCISCO

Approved:

DocuSigned by:
Ashish Raj
13BDA73A066E4E0...

Ashish Raj
Chair

DocuSigned by:
Srikantan Nagarajan
DocuSigned by:45E...

Srikantan Nagarajan

DocuSigned by:
Alastair Martin

Alastair Martin

DocuSigned by:404...
Susanne Mueller
F57F92ED5A53475...

Susanne Mueller

Committee Members

Acknowledgment

I would like to express my deepest gratitude to everyone who made this work possible. I am grateful to my committee chair, ***Dr. Ashish Raj***, for giving me the opportunity to conduct this thesis research and for providing very insightful guidance. To *Dr. Srikantan Nagarajan*: thank you for introducing me to the team, for always coming up with very interesting ideas, and for your guidance. Thank you to *Dr. Susanne Mueller* and *Dr. Alastair Martin* for your thoughtful comments and feedback.

Most importantly, I would like to thank *Dr. Parul Verma* for introducing me to the world of Neural Mass Models and Spectral Graph Model. It's been a wonderful experience to work with her (still working) and to feel included when she asks for my input. Moreover, I would not be doing research in the first place if it were not for my undergrad supervisor, *Dr. Dalia Dasgupta Mandal*, who has always been there for me and encouraged me to pursue research. I am extremely grateful to have someone like her on this very unknown path I am heading down.

Moreover, it's been a wonderful experience to work with *Mr. Nuutti Barron* on this modeling framework as a team, along with all the amazing scientists here at Raj Lab.

To the **MSBI program:** thank you for fostering a collaborative, inclusive environment that supports growth as a scientist. I am especially grateful to all the faculty and staff, and, to name a few, *Dr. Peder Larson* (who left a lasting impression on me), for explaining complex MRI Physics concepts that made me think deeply while standing for more than two hours in every lecture. Moreover, it has been a truly rewarding journey at UCSF with my amazing classmates.

To my family**,** I am deeply grateful for their support and encouragement throughout my academic journey. I would not have come this far without their support, including my uncles.

Spectral Graph modeling of abnormal neural synchronizations in Alzheimer's disease

Apurba Debnath

Abstract

Alzheimer's disease (AD) is the most prevalent form of dementia associated with impaired cognitive ability and abnormal neural synchrony. Electrophysiological studies done by magnetoencephalography (MEG) reveal abnormal neural synchrony, reflected in brain signals with elevated power in the delta-theta band (1-7 Hz) and reduced power in the alpha-beta-gamma band (8-51 Hz), accompanied by altered neural driving activity that is scale-free in nature due to the lack of a dominant temporal scale. However, despite being a fundamental component of brain activity, the role of scale-free neural driving dynamics and their influence on altering brain network organization in AD remains poorly understood. To address this, a biophysical modeling framework called the Spectral Graph Model (SGM) is used in this study to deconvolve the scale-driving signals, analyze how they are altered in AD compared with healthy controls, and examine their effects on excitatory-inhibitory (E/I) neuronal dynamics. MEG recordings from a cohort of 77 AD and 77 healthy control subjects are used in this study. AD is accompanied by altered scale-free driving signals across frequency bands compared to healthy controls, with a significant increase in delta-theta power, especially in the temporo-parietal cortices and frontal cortices; a biphasic pattern in the alpha band with increased power in the medial temporo-parietal and frontal regions and reduced power in the lateral posterior-parietal cortices; the beta band shows reduced power in the lateral posterior-parietal cortices, while the gamma band shows an

overall reduction in power across brain regions. These spatial patterns of altered scale-free driving signals, especially the delta-theta, alpha, and beta bands, recapitulate the AD-vulnerable cortices revealed by hypometabolism, amyloid-beta, and tau accumulation in this AD patients' cohort. Altered scale-free driving signals significantly impaired the temporal profiles of E/I dynamics, with AD showing a significant increase in local and long-range excitatory time constants, reflecting local and global slowing of excitatory neural dynamics. Together, these findings demonstrate that scale-free neural driving signals are profoundly disrupted in AD, contributing to alterations in both local E/I dynamics and long-range inter-regional network dynamics, paving the way for a potential new biomarker of AD.

Table of Contents

List of Figures

List of Tables

1. Introduction

Alzheimer's disease (AD) is one of the most common forms of dementia, which progressively degrades the cognitive ability as well as affects the neural synchrony of the affected individuals. There are various hypotheses regarding AD, such as impaired glymphatic clearance (Nedergaard, M., & Goldman, S. A., 2020), reflecting the accumulation of neurotoxic proteins like β-amyloid and tau, which are hallmark biomarkers of AD (Braak, H., & Braak, E., 1991). However, recent studies reveal that they do not always accurately predict cognitive decline (Dubois et al., 2024), underscoring the need for alternative biomarkers. Electrophysiological studies done by magnetoencephalography (MEG) and electroencephalography (EEG) offer a window in this direction, where AD is associated with abnormal neural synchrony, reflected in the power spectra of brain signals showing elevated delta-theta (1-7 Hz) power and reduced alpha-beta-gamma (8-51 Hz) power (Uhlhaas, P. J., & Singer, W., 2006).

Another aspect of brain signals is arrhythmic or scale-free, or aperiodic brain activity – a component distinct from rhythmic activity that changes dynamically with cognitive states, and follows power-law distribution, where $Power \propto 1/f^{\beta}$ and follows an approximate linear trend in log(power) vs log(frequency) space [$log(Power) \propto -\beta log(f)$], which is what a typical biological system follow, where with the increase in frequency, power decreases (He et al, 2010; He, B. J., 2014). This brain activity is called scale-free due to the absence of a dominant temporal scale and is quantified using the spectral exponent (slope) in the frequency domain. Recently, studies on scale-free/aperiodic brain activity in the context of neurological disorders have gained traction, with clinical studies showing that various disorders are associated with disrupted scale-free activity (Donoghue, T., 2025), including AD (Ranasinghe et al, 2025).

Moreover, quantification of scale-free brain activity using spectral slopes/exponents depends heavily on the frequency range over which they are being calculated, making it difficult to generalize across studies. It thus remains to be investigated how the underlying actual scale-free signals (rather than relying solely on spectral slope) are altered and how they drive or affect excitatory–inhibitory (E/I) interaction dynamics and inter-regional network connectivity, thereby influencing oscillatory brain activity. Hence, it's called scale-free driving signals, as they drive the alteration of E/I dynamics.

Therefore, the hypothesis of this study in the context of AD is that AD pathology is accompanied by altered scale-free driving signals that affect oscillatory brain dynamics. Specifically, the hypothesis is that altered scale-free driving signals disrupt local/regional E/I dynamics and inter-regional network connectivity dynamics, together exhibiting altered oscillatory and scale-free brain activity in AD.

To test this hypothesis, a deconvolution framework is implemented in this study to recover these scale-free/aperiodic driving signals and to model oscillatory brain activity using biophysical model parameters, together capturing the MEG power spectra of every brain region. In this approach, the scale-free biologically plausible driving signals are recovered by following the electrophysiological power-law distribution $1/f^{\beta}$ across the frequency range, having delta-theta-alpha-beta-gamma frequency bands. Using this framework, the deconvolved scale-free driving signals have been examined to compare between AD and healthy controls in various frequency bands, such as delta-theta (1.75-7 Hz), alpha (8-12 Hz), beta (13-30 Hz), gamma (31-51 Hz) bands, and subsequently examined how they affect oscillatory brain activity, as measured by biophysical model parameters.

In this regard, to provide a mechanistic basis for this investigation and the successful deconvolution of scale-free driving signals, a biophysically grounded modeling framework, the Spectral Graph Model (SGM), has been employed, which yields an analytical closed-form solution in the frequency domain (Raj et al., 2020; Verma, P., Nagarajan, S., & Raj, A., 2022). SGM requires only a small set of biophysically interpretable parameters, making it a parsimonious yet powerful framework for studying large-scale brain activity. Critically, the analytical structure of SGM naturally enables the deconvolution and characterization of latent biologically plausible scale-free driving signals. The model captures local E/I population-level dynamics arising from interactions between these two types of neurons within each brain region, while simultaneously incorporating long-range neuronal communication mediated through structural connectivity – white matter pathways. SGM and its local version have been successfully employed in previous Alzheimer's studies, as well as a brain-computer interface study to provide a mechanistic basis for learning dynamics (Ranasinghe et al, 2022; Verma et al, 2024; Debnath et al, 2025). Thus, by integrating local E/I dynamics with global, inter-regional network topology, SGM provides a biophysically interpretable framework for investigating how pathological alterations in scale-free driving signals drive the large-scale network dysfunction and abnormal neural synchrony in AD. The proposed framework of this study is illustrated in **Fig. 1.1**

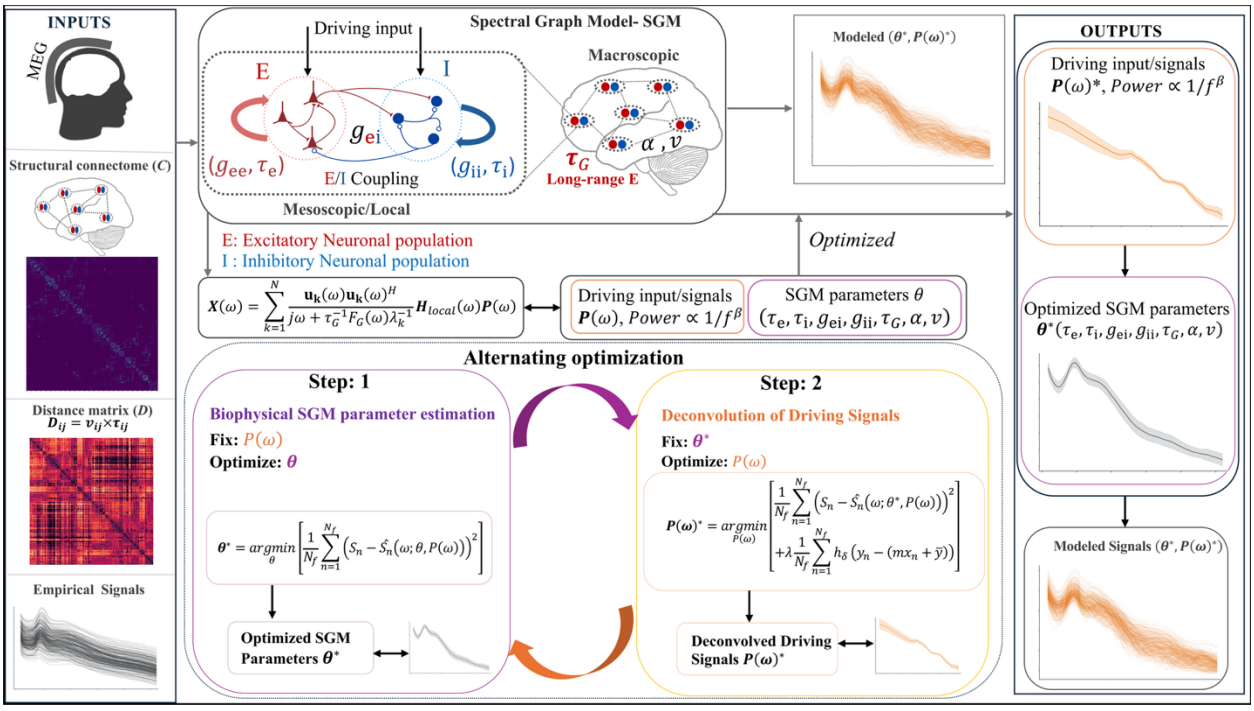

Figure 1.1: Project framework: Spectral Graph Model (SGM) (at the top middle), comprising local excitatory-inhibitory (E/I) neuronal population interaction modeled for each brain region with a driving input, while taking global information such as inter-regional connectivity dynamics through long-range excitatory neuronal population projection. The model takes MEG empirical signals of every region, structural connectivity matrix and distance matrix as a measure of inter-regional connectivity information (shown on the left) and gives output as optimized seven biophysical model parameters capturing oscillatory brain dynamics while deconvolving scale-free driving signals following electrophysiological power law distribution, and together they give modeled signal of every brain region (shown on the right) by doing two step optimization process (implemented in this study), with optimizing seven model parameters in step-1 and deconvolving scale-free driving signals in step-2 following electrophysiological power-law distribution (shown at bottom middle).

2. Materials & Methods

2.1 Participants and MEG data

This study is conducted using a previously published well-characterized cohort of AD patients (n=77; age, 62.6 ± 8.9 years), with CDR scale of 0.5 (n=38) and 1 (n=39), and healthy controls (n=77; age, 65.5 ± 10.4 years). All AD patients met the National Institute of Aging-Alzheimer's Association criteria and were positive for AD biomarkers (CSF or amyloid-PET, or histopathological confirmation at autopsy), and they were examined at the UCSF Memory and Aging Center (UCSF-MAC). The healthy controls (n=77) were recruited from the community and selected for normal cognitive performance, normal MRI, and the absence of neurological, psychiatric, or other major illnesses. Informed consent was obtained from each participant or their assigned surrogates. For more information on AD, please refer to (Ranasinghe et al, 2025; Verma et al, 2024). Power spectra of the source-reconstructed MEG recordings from all subjects have been calculated for the 246 cortical and subcortical regions defined by the Brainnetome atlas.

2.3 Spectral Graph Model (SGM)

SGM used here is built upon the one developed previously (Raj et al, 2020; Verma et al, 2022), which was specified in a closed form in the frequency domain as a function of angular frequency ω. The steady-state frequency response of various brain regions can be solved in closed form using SGM. It is defined by seven biophysically meaningful parameters, which are either global or local but spatially invariant. These parameters, $\boldsymbol{\theta}$ $(\tau_e, \tau_i, g_{ei}, g_{ii}, \tau_G, \alpha, v)$ include the spatially-invariant local synchrony-related time constants: excitatory time constant (τ_e); inhibitory time

constant (τ_i); along with spatially-invariant local neural gains: E/I coupling neural gain (g_{ei}) reflecting strength of recurrent interaction between excitatory and inhibitory neurons at the population level; inhibitory neural gain (g_{ii}) reflecting self-inhibitory neural feedback gain; as well as global parameters: long-range excitatory time constant (τ_G) reflecting the decay time of long-range excitatory neurons' response; long-range connectivity coupling constant (α), and long-range signal transmission speed among regions (v). SGM is characterized by an additional local excitatory neural gain parameter (g_{ee}) , but it is set to 1 to ensure parameter identifiability. Each region is assumed to have local excitatory and inhibitory neuronal subpopulations that interact with one another and regulate long-range excitatory neuronal populations. The long-range populations are assumed to be linked via the structural connectome. Here, 246 brain regions, including cortical and subcortical regions, were considered using the Brainnetome parcellation scheme, and a corresponding structural connectome template from the Human Connectome Project (HCP) was used. As a result, the model includes no features that may vary across regions, except those from the heterogeneously connected anatomical network.

The regional signal accounts for interactions between excitatory (E) and inhibitory (I) neuronal populations and is assumed to be the same across regions. The local model parameters ($g_{ei}, g_{ii}, \tau_e, \tau_i$) regulate $\boldsymbol{H}_{local}(\omega)$ that captures local E/I interactions, and the local regional signals generated from local E/I interactions interact with the long-range excitatory neuronal population and are transmitted to different regions through the structural connectome. From the structural connectome, a complex connectome in the Fourier domain $\boldsymbol{C}^*(\omega)$ is obtained, incorporating time delays in signal transmission across the connectome. The complex Laplacian matrix is defined by, $\boldsymbol{\mathcal{L}}(\omega) = \boldsymbol{I} - \kappa \boldsymbol{C}^*(\omega)$ and, $\boldsymbol{I}$ is the identity matrix of size $N \times N$. The eigen-decomposition of this complex Laplacian matrix is $\boldsymbol{\mathcal{L}}(\omega) = \boldsymbol{U}(\omega)\boldsymbol{\Lambda}(\omega)\boldsymbol{U}(\omega)^{\mathrm{H}}$, where $\boldsymbol{U}(\omega)$ are

the eigenmodes/eigenvectors and $\boldsymbol{\Lambda}(\omega) = \mathrm{diag}([\lambda_1(\omega), \ldots, \lambda_N(\omega)])$ consist of the eigenvalues $\lambda_1(\omega), \ldots, \lambda_N(\omega)$, at angular frequency. Thus, the macroscopic response $\boldsymbol{X}(\omega)$ is obtained as follows:

$$\boldsymbol{X}(\omega) = \sum_{k=1}^{N} \frac{\boldsymbol{u}_k(\omega)\boldsymbol{u}_k(\omega)^{\mathrm{H}}}{j\omega + \tau_G^{-1}\lambda_k(\omega)F_G(\omega)} \boldsymbol{H}_{local}(\omega)\boldsymbol{P}(\omega)$$

where $\boldsymbol{X}(\omega)$ is a vector of signals at every brain region, $\boldsymbol{u}_k(\omega)$ are the eigenmodes, and $\lambda_k(\omega)$ are the eigenvalues obtained by the eigen-decomposition of a complex Laplacian matrix, and $F_G(\omega)$ is the Fourier transform of a Gamma-shaped neural response function. $\boldsymbol{P}(\omega)$ is a vector of driving signal of all regions, which is a driving input to the local excitatory and inhibitory neuronal populations, and N is the 246 brain regions.

Therefore, to infer seven SGM parameters and deconvolve the driving signals, this study employs an alternating two-step optimization procedure. In the first step, SGM parameters were estimated by fitting the SGM output to the power spectral density (PSD) of MEG recordings of all regions, subjects in AD, and the healthy control cohort. In the second step, the remaining biologically plausible signals were recovered through deconvolution by allowing their power to follow the power-law form $1/f^{\beta}$.

2.4 Mathematical modeling

2.4.1 Parameter estimation and deconvolution of driving signals

Modeling framework SGM, derived from 7 biophysically interpretable parameters are constrained within biologically plausible bounds based on prior experiments, model stability analysis and recent evidence (Raj et al, 2020; Verma et al, 2023; Verma et al, 2024; van Blooijs

et al, 2023), and shown in Table 2.4.1. Thus, to infer/estimate these model parameters and deconvolve biologically plausible scale-free neural driving signals from empirical PSDs of each region and subject, an iterative modeling framework has been implemented in this study. This modeling framework alternates between estimating 7 SGM parameters and deconvolving the driving signals. To enable unconstrained optimization while preserving parameter bounds, the parameters were transformed into a latent space via a logit transformation $\left(\theta_{scaled} = \ln\left(\frac{\theta-\theta_{min}}{\theta_{max}-\theta}\right)\right)$. Optimized parameters were subsequently mapped back to the original parameter space using the inverse sigmoid transformation. The optimization procedure was initialized with initial values, and the driving input spectrum $P(\omega)$ was initialized as a complex signal: $P(\omega) =$ 0.5 + 0i, for all 246 brain regions and frequencies. The optimization settings include: number of alternating optimization rounds = 2; parameter inference epochs per round = 30; deconvolution epochs per round = 10; learning rates for parameter inference and deconvolution are 0.01 and 0.1, respectively. Prior to optimization, empirical PSDs were scaled to stabilize training and maintain comparable scaling across regions and frequency, as $PSD_{scaled} = \frac{PSD}{\sum PSD}$

Alternate Optimization. In this study, two-step alternating optimization was implemented for each subject across all 246 brain regions in both the AD and healthy control cohorts, comprising 77 subjects in each cohort. In step 1, seven SGM Parameters ($\boldsymbol{\theta}$) were estimated/optimized, and in step 2, the driving signals $P(\omega)$ were deconvolved for all regions, subjects, and cohorts. During the first optimization round, it $P(\omega)$ was not used for parameter estimation, allowing the model to first estimate a global scaling factor and coarse parameter configuration. In the subsequent round, the deconvolved $P(\omega)$ signals obtained from deconvolution were held fixed in parameter estimation. That way, it's done for two rounds, comprising these two steps.

Step - 1: SGM parameter estimation. In this step, for fixed initial $P(\omega)$, 7 SGM parameters (θ) were optimized in their respective bounds after initialization (as shown in Table 2.4.1) using the Adam optimizer, and the modeled power spectra were fitted to the empirical power spectra using Mean-Squared Error (MSE) as a loss function such as,

$$\theta^* = \underset{\theta}{argmin}\left[\frac{1}{N_f}\sum_{n=1}^{N_f}\left(S_n - \hat{S_n}\left(\omega;\theta,P(\omega)\right)\right)^2\right]$$

where S_n and $\hat{S_n}\left(\omega;\theta,P(\omega)\right)$ are the observed and modeled PSDs at the n-th frequency bin respectively, and N_f is the number of frequency bins. In this step, $P(\omega)$ is fixed while the SGM parameters θ are optimized to obtain θ^* and the optimization was performed for 30 epochs. After optimization, parameters were mapped back to their original parameter space using the inverse sigmoid transformation.

Step - 2: Deconvolution of driving signals. Following parameter estimation in step 1, in this step, driving signals $P(\omega)$ are deconvolved while the optimized parameters (θ^*) from step 1 are held fixed. As in step 1, the Adam optimizer is used in this step as well, and the signals are deconvolved using MSE as the loss function and an additional regularization loss – the Huber loss with a regularization weighting $(\lambda = 206,\ \ from\ L - sweep)$. This latent spectrum was modeled as a complex-valued regional and frequency-dependent signal. To deconvolve physiologically plausible scale-free neural driving signals, the deconvolved signals were regularized using the electrophysiological power-law distribution $1/f^{\beta}$ across the frequency range in the log-log domain, by minimizing the Huber loss between the deconvolved signals' log-power spectrum and the corresponding target approximate linear trend in log (power) vs log (frequency) space as,

$$P(\omega)^* = \underset{P(\omega)}{argmin}\left[\frac{1}{N_f}\sum_{n=1}^{N_f}\left(S_n - \hat{S_n}\left(\omega;\theta^*,P(\omega)\right)\right)^2 + \lambda\frac{1}{N_f}\sum_{n=1}^{N_f}h_\delta\left(y_n - (mx_n + \bar{y})\right)\right]$$

where the power of the deconvolved signals at the n-th frequency bin in log-scale, is:

$$y_n = \log_{10}\left(|P(\omega_n)|^2\right)$$

And the target biologically plausible approximate linear scale-free driving signal in the log (power) vs log (frequency) space from the power-law distribution [$\log(power) \propto m\log(frequency)$] is:

$$mx_n + \bar{y}$$

where,

$$m = \frac{\sum_{n=1}^{N_f} x_n\,(y_n - \bar{y})}{\sum_{n=1}^{N_f} x_n^2}, \quad x_n = \log_{10}(f_n) - \overline{\log_{10}(f)}\,, \quad \bar{y} = \frac{1}{N_f}\sum_{n=1}^{N_f}\log_{10}\left(|P(\omega_n)|^2\right)$$

and the Huber loss function on a residual (a), between the log (power) of the deconvolved signals and target linear driving signals, defined by $h_\delta(a)$ such that:

$$h_\delta(a) = \begin{cases} \frac{1}{2}a^2, & |a| \le \delta, \\ \delta\left(|a| - \frac{1}{2}\delta\right), & |a| > \delta, \end{cases}$$

The parameter/threshold, δ controls the transition between quadratic behavior for small residuals ($|a| \le \delta$) and linear behavior for large residuals ($|a| > \delta$), thereby improving robustness to outliers, and is set to 1 by default in *PyTorch*. Note that the Huber loss function is implemented using the *PyTorch* deep learning library via the module `torch.nn.HuberLoss`.

L-Curve sweep To get the optimal regularization weight (λ), an L-sweep for 20 points in log-space between $(10^0 - 10^4)$ was done for all subjects and the maximum curvature method was used to get the optimal/corner value of (λ) using the average MSE Loss (ρ) and regularization-Huber loss (η) across subjects in both AD and control cohorts. The curvature $\kappa(\lambda)$ of the L-curve $(\hat{\rho} = \log\rho\,, \hat{\eta} = \log\eta)$ in the log-log scale can be defined by (Hansen & O'Leary, 1993),

$$\kappa(\lambda) = \frac{\hat{\rho}'\hat{\eta}'' - \hat{\rho}''\hat{\eta}'}{[(\hat{\rho}')^2 + (\hat{\eta}')^2]^{3/2}}$$

where $\hat{\rho}',\ \hat{\rho}'',\ \hat{\eta}' and\ \hat{\eta}''$ denotes the 1st and 2nd order differentiation of $\hat{\rho}, \hat{\eta}$ with respect to λ, respectively, and the optimal regularization weight λ corresponds to the maximum curvature $\kappa(\lambda)$.

Table 2.4.1: Model parameters with biophysically realistic initial guesses and bounds for estimating the spectra.

Model Parameters	Symbol	Initial guess	Lower/upper bound for optimization
Excitatory Time Constant (ms)	τ_e	17.5 ms	[5.0 ms, 30.0 ms]
Inhibitory Time Constant (ms)	τ_i	175 ms	[5.0 ms, 200 ms]
E/I Coupling Neural gain (arb unit)	g_{ei}	0.25	[0.001, 0.7]
Inhibitory Neural gain (arb unit)	g_{ii}	0.025	[0.001, 2]
Long-range Excitatory Time constant (ms)	τ_G	10 ms	[5.0 ms, 30 ms]
Long-range Transmission Speed (m/s)	v	17 m/s	[1.0 m/s, 20.0 m/s]
Long-range Connectivity Coupling Constant (arb unit)	α	0.5	[0.1, 1]

2.5 Model evaluation, and statistical analyses

To analyze model performance, two metrics were used to evaluate the modeled spectra against empirical spectra: Pearson correlation and root-mean-squared error (RMSE), across all regions and subjects in both the AD and control cohorts. Next, to analyze the signals' power difference at the group-level for AD vs. Controls in different frequency bands, analysis of covariance was implemented while taking age as a covariate, and false discovery rate (FDR) correction was applied for each of the brain regions for multiple comparisons, while setting the significance threshold at 0.05 ($pFDR<0.05$). Thereafter, to analyze differences in parameter distributions at the group level for AD vs. Controls, Mann-Whitney U test was applied and adjusted for multiple comparisons using the Bonferroni correction by setting the significant threshold at 0.05. Similarly, to compare within-group differences between two conditions, the Wilcoxon signed-rank test was applied and adjusted for multiple comparisons using the Bonferroni correction, with a significance threshold of 0.05.

3. Results

3.1 SGM accurately captures MEG power spectra across AD and healthy control subjects

SGM, derived from seven biophysically interpretable parameters that capture oscillatory activity, together with deconvolved scale-free driving signals, accurately captured the MEG power spectra of all 246 cortical/subcortical regions across all subjects in both AD and healthy control groups. To qualitatively illustrate model performance, representative empirical and corresponding modeled spectra (Z-score normalized) having oscillatory and scale-free neural activity of all brain regions, subjects (Controls, AD) are shown in Fig. 3.1-(A, B) and corresponding modeled signals in Fig. 3.1- (C, D), reflecting a close alignment in spectral profiles across the examined frequency range, highlighting the ability of the SGM to reproduce region-specific spectral characteristics. Quantitative analysis between the modeled and empirical PSDs across all regions and subjects demonstrated a strong correspondence in the decibel (dB) scale over the frequency range of [1.75–51 Hz], comprising delta-theta-alpha-beta-gamma bands, where the Pearson correlation exceeded 0.80 with RMSE less than 0.4 for most regions and subjects considered in this study (Fig. 3.1-G, H). Moreover, the modeled spectra successfully reproduced the characteristic abnormal neural synchrony observed in AD patients, including elevated power within the delta–theta frequency range (2–7 Hz) and reduced power within the alpha–beta-gamma frequency range (8–51 Hz) relative to healthy controls, as shown in Fig. 3.2. Note that two rounds of alternating optimization were sufficient to achieve optimal results.

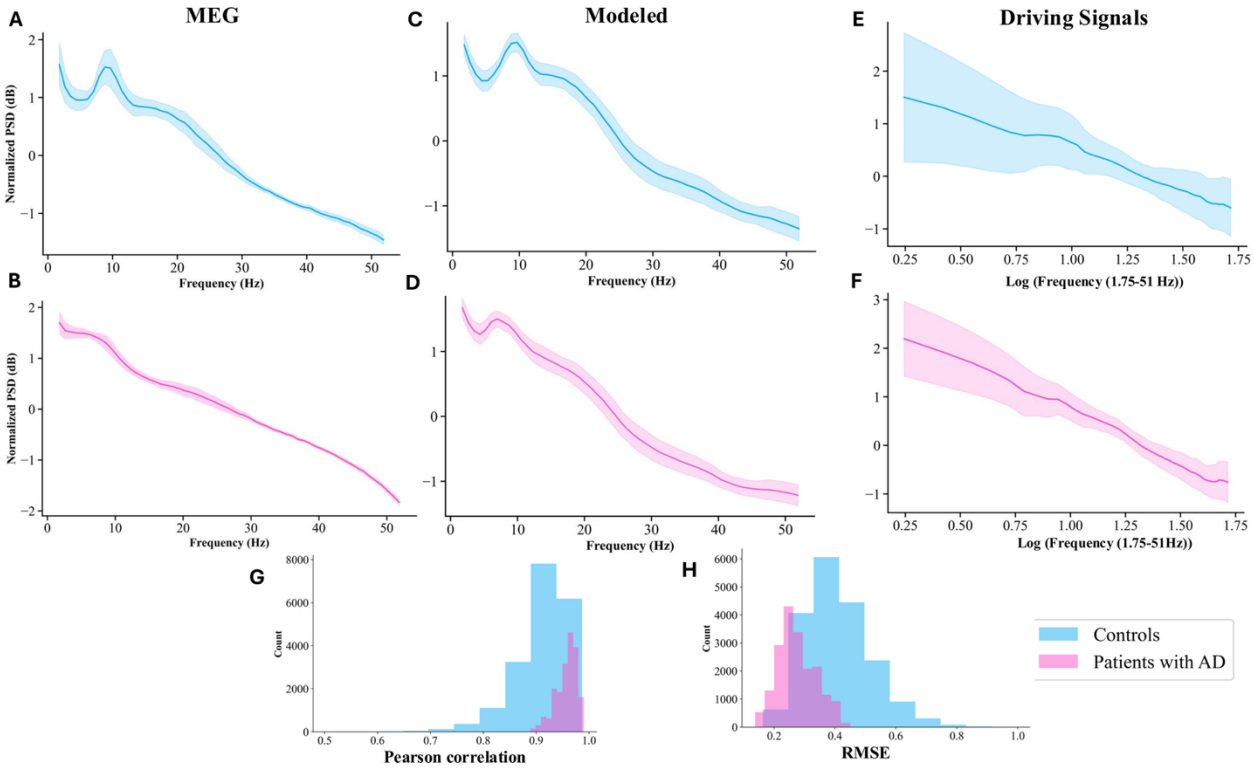

Figure 3.1: SGM accurately captured oscillatory brain activity and deconvolved scale-free driving signals. Plots (A, B) show empirical MEG power spectra for all regions and subjects in the healthy controls and AD cohorts, respectively, and the corresponding modeled spectra are shown in (C, D), having oscillatory and scale-free deconvolved driving signals shown in (E, F). Plot (G, H) shows the Pearson correlation and RMSE between the modeled and empirical power spectra across all regions and subjects in both the controls and AD cohorts, indicating that, for most regions, the Pearson correlation exceeded 0.80, with RMSE values less than 0.5 in 90% of regions.

3.2 Deconvolved scale-free neural driving signals are significantly disrupted in AD

The deconvolved scale-free neural driving signals, reflecting neuronal driving input in each neural mass at every brain region that follows an electrophysiological power-law form $1/f^{\beta}$, exhibited marked alterations in AD patients compared to healthy controls in different frequency bands for different regions, as illustrated by the spatial patterns of the power in Fig. 3.2, where the positive t-values (red) from the analysis of covariance (taking age as a covariate) reflect high power in AD compared to healthy controls, whereas negative t-values reflect reduced power in AD compared to healthy Controls. All regions are FDR-corrected for multiple comparisons with pFDR < 0.05. Group-level Analysis for AD vs. Controls revealed that AD pathology is accompanied by a significant increase in scale-free neural driving signals' power in the delta-theta (1.75- 7 Hz) band in the medial temporo-parietal cortex areas and frontal areas; while the alpha band (8-12 Hz) shows increased power in medial temporo-parietal, and inferior frontal regions, with the reduced power in the lateral posterior-parietal cortex in AD patients. The beta band (13-30 Hz) shows only reduced power in the lateral posterior-parietal cortex, whereas the gamma band (31-51 Hz) shows no region-specific variation in AD; it is accompanied by a global reduction in power across all regions.

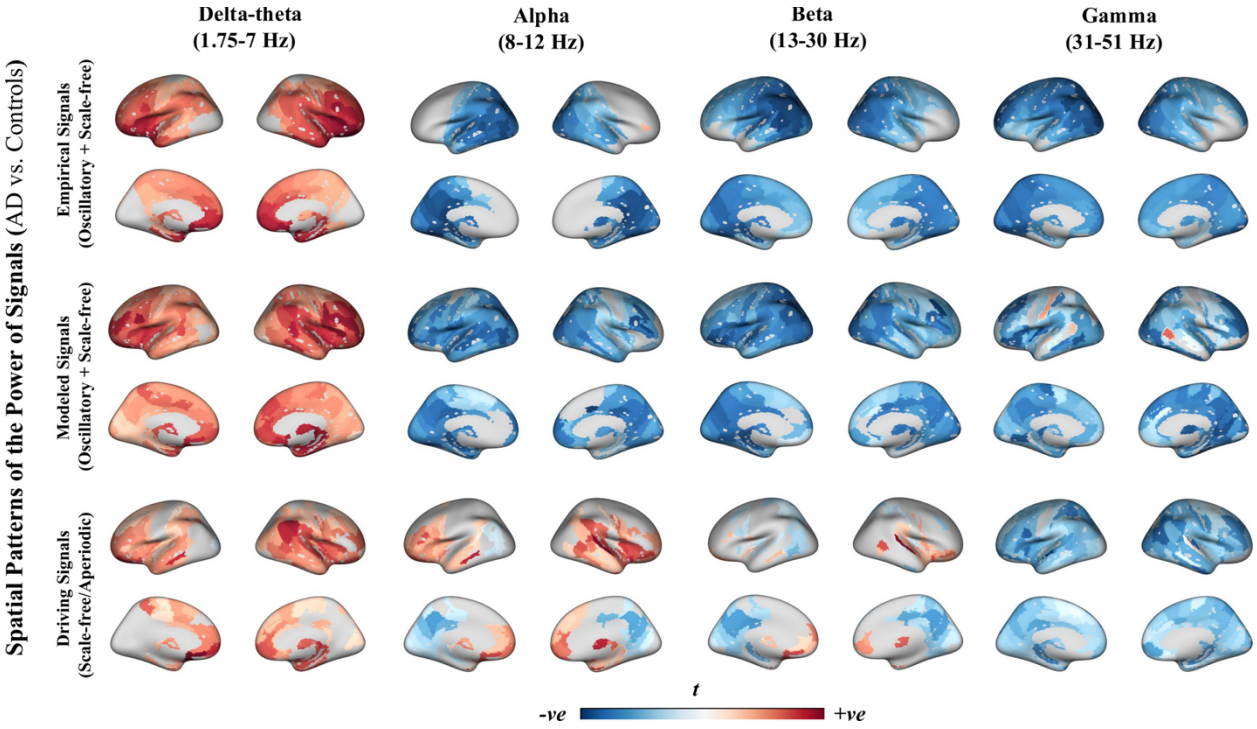

Figure 3.2: Significant alteration in the power of signals in AD compared to healthy controls. Spatial patterns of t-values show the power of signals in different brain regions for AD vs. Control, from analysis of covariance, with age as a covariate (FDR-corrected $p < 0.05$). A positive t-value indicates higher AD power, whereas a negative value indicates lower AD power compared to controls. The top row shows the spatial patterns of group differences (AD vs Controls) in the power of empirical MEG signals across different frequency bands (delta-theta, alpha, beta, and gamma), with the corresponding modeled signals shown in the second row. Both the empirical and modeled spectra show elevated delta-theta (1.75-7 Hz) band power in AD, with reduced alpha-, beta-, and gamma-band (8-51 Hz) power. The third row shows the spatial patterns of the power of deconvolved scale-free driving signals in different frequency bands. It shows that elevated delta-theta (1.75-7 Hz) power in temporo-parietal and frontal cortices in AD; biphasic patterns in alpha (8-12 Hz) band power, with the increased power in lateral temporo-parietal and inferior frontal cortices and reduced power in medial posterior-parietal cortices; reduced beta (13-30 Hz) band power in in medial posterior-parietal cortices, with the global reduction in the gamma (31-51Hz) power across regions.

3.3 AD is associated with alterations in local E/I neuronal dynamics and inter-regional connectivity dynamics

Biophysical measures of the local (regional) E/I dynamics and long-range inter-regional connectivity dynamic demonstrate significant alterations in AD (CDR=05 & CDR=1) compared to healthy control subjects at the group level, clearly shown in in Fig. 3.3. In particular, the temporal profiles are significant disrupted in AD compared to controls, reflected by the significant increase in local excitatory time constant (τ_e) (Fig. 3.3-A, Mann-Whitney U test, Bonferroni corrected $p < 10^{-6}$), indicating prolonged regional excitations in AD, along with significant modulation of the local inhibitory time constant (τ_i) between the two groups (Fig. 3.3-B), with the healthy control showing much more inter-subject heterogeneity. Moreover, regional E/I coupling neural gain also revealed significant alterations in AD relative to controls (Fig. 3.3-C), reflecting disrupted recurrent interactions between E/I neuronal populations, with healthy controls again exhibiting much more heterogeneity. In contrast, inhibitory neural gain (g_{ii}), reflecting self-inhibitory neural feedback gain, does not show any significant difference between AD and healthy controls (Fig. 3.3-D, Mann-Whitney U test, Bonferroni corrected $p > 0.05$), implying that inhibitory neuronal population's interactions remain relatively preserved. Additionally, at the global level, i.e., with long-range inter-regional connectivity, the long-range excitatory time constant (τ_G) exhibited a significant elevation in AD, especially in the early Alzheimer's patients with CDR=1 (E) (Fig. 3.3-E: Controls vs CDR=1, Mann-Whitney U test, Bonferroni corrected $p < 0.0001$), reflecting slower long-range excitatory dynamics. However, long-range signal transmission speed did not differ between AD and healthy controls (Fig. 3.3-F, Mann-Whitney U test, Bonferroni-corrected $p > 0.05$). Meanwhile, the long-range inter-regional connectivity coupling constant (α) shows a weak group difference when comparing healthy

controls with CDR=1 (Fig. 3.3-G). Importantly, no parameters showed significant differences between the CDR=0.5 and CDR=1 AD sub-groups.

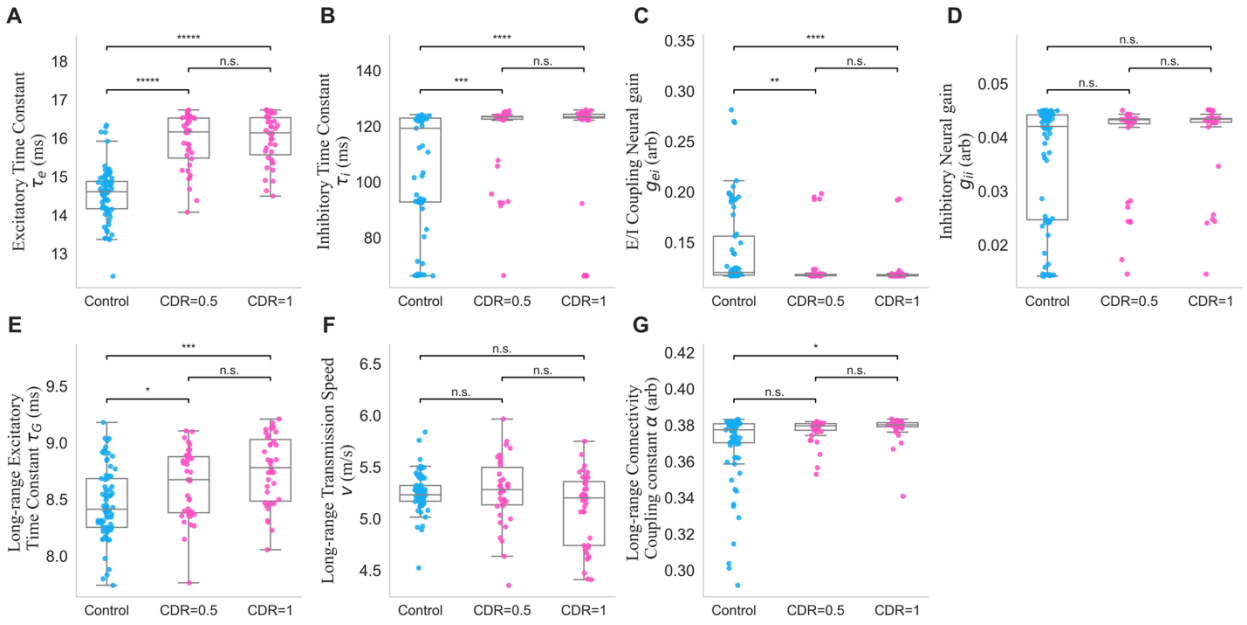

Figure 3.3: AD is accompanied by alterations in local E/I dynamics and inter-regional network connectivity dynamics. (A-D) Local E/I dynamics measure: Excitatory (A, τ_e) and inhibitory (B, τ_i) time constants are significantly elevated in AD (CDR=0.5 & CDR=1) compared to Controls; Neural gains, E/I coupling gain (C, g_{ei}) is significantly reduced in AD compared to Controls, but it's not that apparent, as Controls show much more heterogeneity and Inhibitory gain (D, g_{ii}) does not differ significantly between AD and controls. (E-G) long-range inter-regional connectivity dynamics: Long-range excitatory time constant (E, τ_G) shows that with the increase in cognitive decline (CDR=1) in AD, the global slowing becomes much more apparent as reflected by a significant increase in their values and, other long-range parameters such as transmission speed (F, v) remains unchanged across groups and inter-regional connectivity coupling constant (G, α) does not show any apparent difference between AD and Controls. Comparisons between CDR=0.5 and CDR=1 are not significant for any parameter. Each point represents an individual subject in all box plots. Statistical significance was assessed using the Mann-Whitney U test with Bonferroni correction for multiple comparisons, $*: p < 0.05, **: p < 0.005, ***: p < 0.0001, ****: p < 0.00001, *****: p < 0.000001, n.s., not\ significant.$

3.4 Deconvolved scale-free driving signals significantly alters biophysical model parameters in AD

Next, to analyze the effect of deconvolved scale-free driving signals on the seven biophysical model parameters in the step 2 condition, compared to the step 1 condition with the fixed input ($P(\omega)$), a comparison is made within each cohort under these two conditions. Scale-free driving signals produced significant changes in nearly all estimated biophysical parameters. Within-group comparisons in AD demonstrated significant alterations across all local and global neuronal measurements (Fig. 3.4: A-G). At the local level, scale-free driving signals were associated with a significant increase in excitatory (τ_e) and inhibitory (τ_i) time constants (Fig. 3.4: A, B). In contrast, E/I coupling neural gain (g_{ei}) was significantly reduced under (Fig. 3.4-C), whereas the inhibitory neural gain (g_{ii}), reflecting self-inhibitory neural feedback gain, was significantly increased (Fig. 3.4-D). At the global level, scale-free driving signals produced a significant increase in the long-range excitatory time constant (τ_G) (Fig. 3.4-E) and long-range inter-regional connectivity coupling constant (α) (Fig. 3.4-G), while long-range transmission speed (v) does not differ between these two conditions and showed heterogeneity (Fig. 3.4-F). All the Statistical significance was assessed using the Wilcoxon signed-rank test with Bonferroni correction for multiple comparisons, $*: p < 0.05, **: p < 0.005, ***: p < 0.0001, ****: p < 0.00001, *****: p < 0.000001, n.s., not\ significant$.

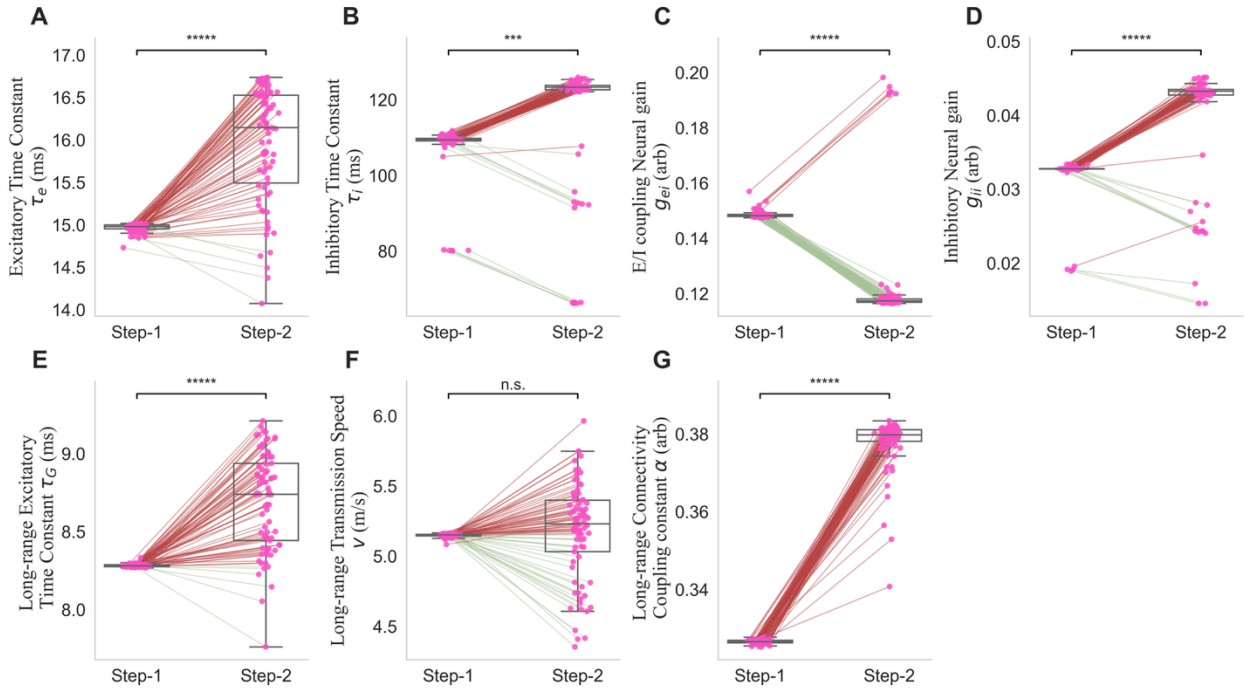

Figure 3.4: Effect of deconvolved scale-free driving signals on biophysical model parameters in AD. Within the AD cohort, estimated model parameters under deconvolved scale-free driving signals (Step-2) are compared with those obtained with fixed input $\big(P(\omega)\big)$(Step-1). (A-D) Local E/I dynamics: scale-free driving signals significantly increase the excitatory (A, τ_e) and inhibitory (B, τ_i) time constants, while significantly decreasing and increasing E/I coupling neural gain (C, g_{ei}) and inhibitory neural gain (D, g_{ii}), respectively. (E-G) inter-regional network connectivity dynamics: scale-free driving signals significantly increase long-range excitatory time constant (E, τ_G) and long-range inter-regional connectivity coupling constant (G, α), whereas the long-range transmission speed (F, v) showed heterogeneity. Here, the line connects paired estimates from the same subject, with each point representing an individual subject in all box plots. Statistical significance was assessed using the Wilcoxon signed-rank test with Bonferroni correction for multiple comparisons, $*: p < 0.05, **: p < 0.005, ***: p < 0.0001, ****: p < 0.00001, *****: p < 0.000001, n.s., not\ significant.$

3.5 Healthy controls exhibited heterogeneous E/I modulations under deconvolved scale-free driving signals

In contrast to AD, within-group comparisons in healthy control subjects showed weaker and less consistent modulation of local E/I parameters under scale-free driving signals in step-2, although the overall trends in global parameters remained similar, as reflected by τ_G, v, α (Fig. 3.5, E-G). One interesting trend is observed with the local excitatory time constant (τ_e), it showed a significant reduction as opposed to AD under scale-free driving signals (Fig. 3.5-A, Wilcoxon test, Bonferroni-corrected $p < 0.001$), whereas the inhibitory time constant (τ_i) does not show any significant difference, accompanied by heterogeneous changes across subjects (Fig. 3.5-B, Wilcoxon test, Bonferroni-corrected $p > 0.05$). Similarly, the E/I coupling neural gain (g_{ei}) does not show any change (Fig. 3.5-C, Wilcoxon test, Bonferroni-corrected $p > 0.05$), with inter-subject heterogeneity. In contrast, inhibitory neural gain (g_{ii}) was significantly elevated in most subjects (Fig. 3.5-D, Wilcoxon test, Bonferroni-corrected $p < 10^{-5}$). Although local neuronal modulation was less pronounced in controls, the global parameters showed trends similar to those observed in AD, including increased long-range excitatory time constants, increased transmission speed, and inter-regional connectivity coupling constant (Fig. 3.5, E–G).

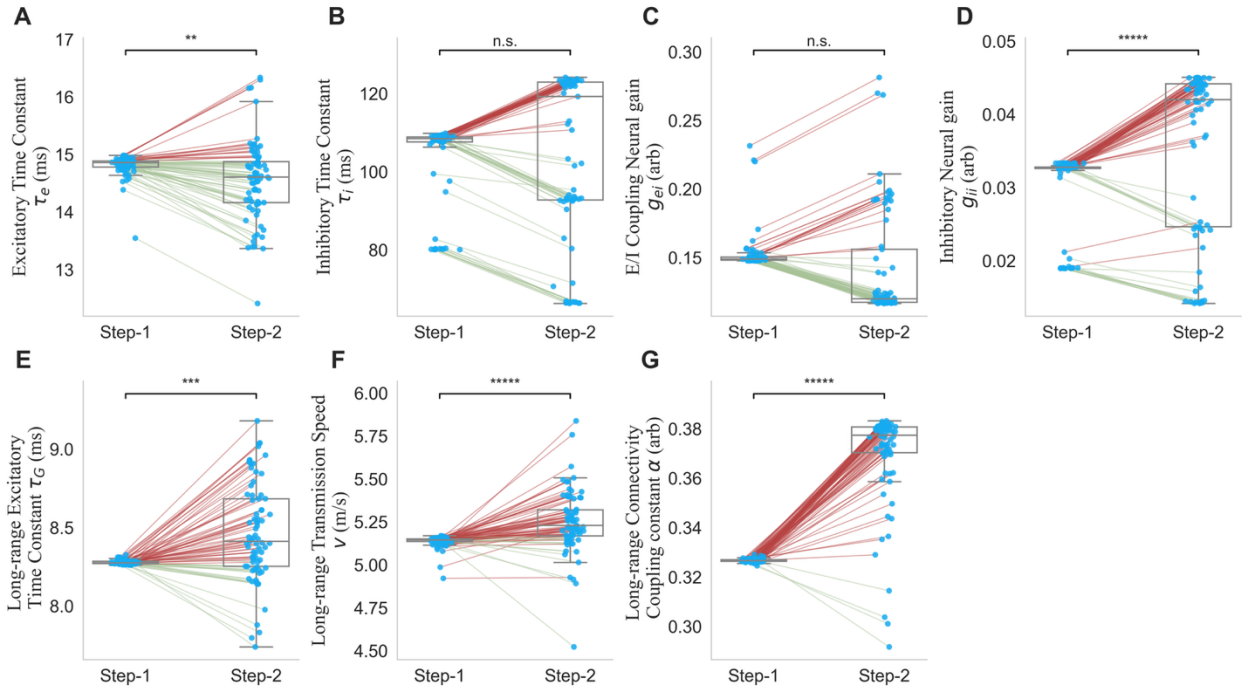

Figure 3.5: Effect of deconvolved scale-free driving signals on biophysical model parameters in healthy Controls. Within the healthy control cohort, estimated model parameters under deconvolved scale-free driving signals (Step-2) are compared with estimates obtained with the fixed input $\big(P(\omega)\big)$(Step-1). Local E/I dynamics (A-D): The excitatory (A, τ_e) significantly reduced under scale-free driving signals, whereas inhibitory (B, τ_i) time constants and E/I coupling neural gain (C, g_{ei}) show substantial inter-subject heterogeneity with no significant paired difference at the group level. In contrast, inhibitory neural gain (D, g_{ii}) is significantly increased. At the global level, i.e., with inter-regional connectivity dynamics (E-G): scale-free driving signals produced a consistent and significant increase in long-range excitatory time constant (E, τ_G), long-range transmission speed (M, v) and long-range inter-regional connectivity coupling constant (G, α). Here, the line connects paired estimates from the same subject, with each point representing an individual subject in all box plots. Statistical significance was assessed using the Wilcoxon signed-rank test with Bonferroni correction for multiple comparisons, $*: p < 0.05, **: p < 0.005, ***: p < 0.0001, ****: p < 0.00001, *****: p < 0.000001, n.s., not\ significant$.

3.6 Excitatory temporal dynamics are selectively amplified in AD at the local and global levels

Next, to determine whether the E/I parameter modulation induced by scale-free driving signals (Step 2) differed significantly between AD and healthy controls, and to compare the actual modulation under scale-free driving signals between AD and controls, a comparison was conducted by computing the difference between Step 2 and Step 1 conditions. The parameter shifts/differences (Δ) are defined as the difference between Step-2 and Step-1 conditions for all biophysical model parameters within the group. Among the local neuronal parameters, the change in the excitatory time constant was significantly greater in AD than in controls (Fig. 3.6-A, Mann–Whitney U test, Bonferroni-corrected $p < 10^{-6}$), indicating that scale-free driving signals drive substantially stronger slowing of local excitatory dynamics in AD. In contrast, no other local neuronal parameters showed significant apparent group differences (Fig. 3.6, B–D), with controls exhibiting much more inter-subject heterogeneity. At the global level, with long-range inter-regional connectivity, the long-range excitatory time constant ($\Delta\tau_G$) demonstrated comparatively modest group differences between the mild-cognitive impairment stage (CDR=0.5) and controls (Fig. 3.6-E: CDR=0.5 vs Controls, Mann–Whitney U test, Bonferroni-corrected $p < 0.05$), and with the early Alzheimer's stage (CDR=1), the global dysfunction becomes much more pronounced with a significant increase in long-range excitatory neural response (Fig. 3.6-E: Controls vs CDR=1, Mann–Whitney U test, Bonferroni-corrected $p < 0.0001$). In contrast, long-range transmission speed (Δv) exhibited no significant differences between the two groups (Fig. 3.6-F, Mann–Whitney U test, Bonferroni-corrected $p > 0.05$), along with weaker modulation in the long-range connectivity coupling constant ($\Delta\alpha$) between controls

and CDR=1 and no difference between controls and CDR=0.5 (Fig. 3.6-G, Mann–Whitney U test, Bonferroni-corrected: Controls vs CDR=0.5, $p > 0.05$; Control vs CDR=1, $p < 0.05$).

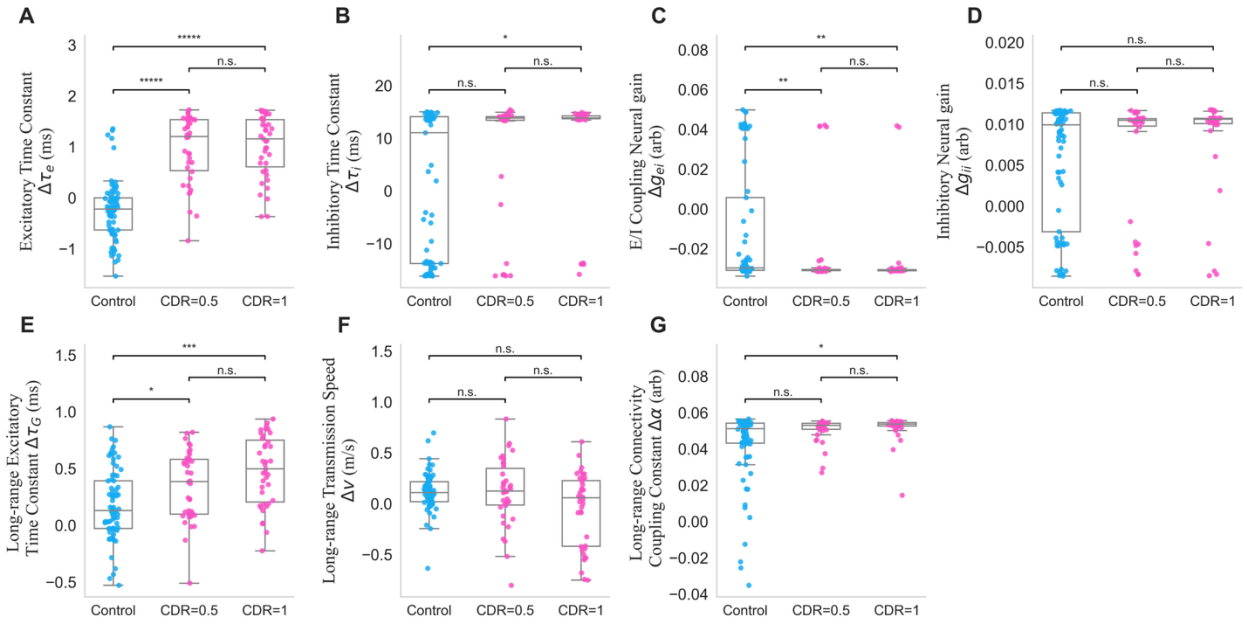

Figure 3.6: AD shows a significant increase in the local and long-range excitatory time scales compared to controls under scale-free driving signals. The change in parameter under scale-free driving signals (step-2), when comparing the difference between step-2 and step-1 ($\Delta = step\ 2 - step\ 1$) for AD vs. controls at the group level, shows that AD is accompanied by a significant increase in excitatory time constant (A, $\Delta\tau_e$) under scale-free driving signals compared to healthy controls, and a significant increase in the long-range excitatory time constant (E, $\Delta\tau_G$), with the strongest group difference observed in the CDR=1 compared to healthy controls. Apart from these two excitatory temporal profiles, no other parameters show apparent significant modulation under scale-free driving signals when comparing AD vs Controls, except for E/I coupling neural gain, which shows significant modulation in AD, but the controls show much more inter-subject heterogeneity. Here as well, comparisons between CDR=0.5 and CDR=1 showed no significant differences in any parameter. Each point represents an individual subject in all box plots. Statistical significance was assessed using the Mann-Whitney U test with Bonferroni correction for multiple comparisons, $*: p < 0.05, **: p < 0.005, ***: p < 0.0001, ****: p < 0.00001, *****: p < 0.000001, n.s., not\ significant$.

4. Discussions

To the best of my knowledge, this is the very first study in which biologically plausible scale-free signals have been deconvolved and analyzed to determine how they change under diseased condition and to assess their effect on oscillatory brain activity, as measured by biophysical model parameters. All previous empirical studies have primarily relied on the spectral slope to quantify scale-free brain activity, which is inherently sensitive to the frequency range analyzed, limiting its generalizability across studies. Therefore, by explicitly analyzing the actual scale-free driving signals, this study provides a new insight into the altered neural synchronization observed in AD, paving the way for a potential new biomarker of AD.

Spatial patterns of the power of deconvolved scale-free driving signals recapitulate AD-vulnerable cortical regions Spatial patterns of the altered power of deconvolved scale-free driving signals in AD show substantial correspondence with cortical regions vulnerable to AD-related metabolic dysfunction, amyloid-beta ($A\beta$) deposition, and tau accumulation. Across frequency bands, especially delta-theta, alpha, and beta, the strongest alterations in AD have been observed in the temporoparietal and frontal association cortices, which broadly overlap regions previously implicated by molecular imaging studies using ^{18}F-FDG, ^{11}C-PIB, and ^{18}F-Flortaucipir, clearly shown in Fig. 4.1- A, B.

In the delta-theta range (1.75–7 Hz), AD showed a significant increase in scale-free driving-signals' power, especially in temporoparietal and frontal regions, whereas alpha band (8–12 Hz) exhibited increased power in inferior frontal regions but reduced power in medial posterior parietal regions, while the beta band (13–30 Hz) showed predominantly reduced power in medial posterior parietal regions. In contrast, the gamma band (31–51 Hz) did not exhibit a distinct

region-specific pattern but instead showed a widespread reduction in power across the cortex (Fig. 4.1, A). This frequency-dependent scale-free driving signals' spatial power organization broadly corresponds to regions characterized by hypometabolism observed by ^{18}F-FDG uptakes in AD, especially in the posterior temporoparietal cortices; Aβ accumulation by ^{11}C-PIB uptake in the medial and dorsolateral cortices of frontal and temporal lobes, as well as regional tau accumulation by ^{18}F-Flortaucipir in the temporoparietal cortices, inferior temporal, temporoparietal junction, and posterior medial parietal cortices (Fig.4.1, B). Altogether, the scale-free driving activity in the delta-theta, alpha, and beta bands recapitulates the regions showing AD-related affect, as measured by molecular imaging studies in this AD population, whereas the gamma band provides no additional information and shows a global reduction in power across brain regions.

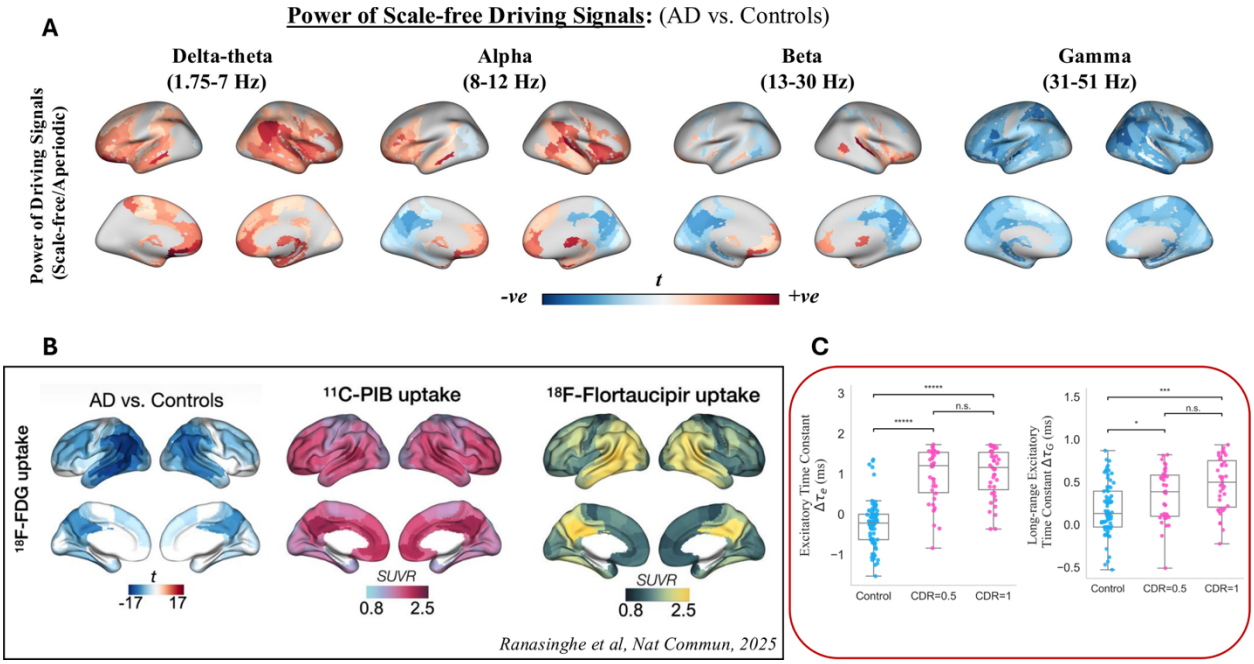

Figure 4.1: Spatial pattern of the power of deconvolved scale-free driving signals recapitulates AD-vulnerable regions. Plot A shows the power of deconvolved scale-free driving signals, especially the delta-theta, alpha, and beta frequency bands, which reflect regions showing AD-related pathological alterations in the bottom box (B) (Ranasinghe et al., Nat Commun 2025). The combination of delta-, theta-, alpha-, and beta-band activity recapitulates alterations observed in AD patients with F-18 FDG, C-11 PIB, and F-18 (tau) uptake in regions such as the temporo-parietal cortex, posterior parietal cortex, and prefrontal cortex. Importantly, the gamma band does not reflect any special information about hyper-metabolism, Aβ, and tau accumulations. Plot C shows the altered scale-free driving signals associated with significantly increased excitatory time constants in AD at the local and global level (long-range).

Excitatory neuronal population activity dominates under frequency-dependent scale-free driving signals Altered scale-free driving signals in AD significantly disrupt oscillatory brain dynamics, as reflected by a significant increase in the local excitatory time constant, implicating prolonged excitatory dynamics (Fig. 4.1- C). Additionally, the long-range excitatory time constant revealed that, with the severity of cognitive decline (CDR=1), this effect becomes much more pronounced at the global level with a significant increase in long-range excitatory time constant under scale-free driving signals, a pattern also observed in the previous SGM study on

Alzheimer's without any deconvolution (Verma et al., 2024). However, under frequency-dependent scale-free driving signals, no parameters of the inhibitory neuronal population show any apparent differences between AD and Controls, potentially indicating that inhibitory neuronal population interactions remain relatively preserved, with excitatory neuronal population activity dominating, implicating local and global slowing of excitatory dynamics.

Limitations One of the limitations of the study is the spatial invariant local parameters across brain regions. This assumption preserves the parsimonious nature of SGM but overlooks regional heterogeneity in the local E/I neural dynamics. A local version of SGM is also available in which four mesoscopic parameters are estimated separately for each region, but it's beyond the scope of this study.

Conclusions

In conclusion, this study demonstrates that biophysical spectral graph modeling can deconvolve latent scale-free neural driving signals from MEG spectra, providing a mechanistically informed characterization of impaired E/I dynamics in Alzheimer's disease. The deconvolved signals exhibited spatial and frequency-specific alterations that broadly aligned with regions affected by Alzheimer's pathology, while the underlying biophysical changes suggested slower excitatory dynamics. These findings highlight deconvolved scale-free neural driving signals as promising candidate biomarkers for capturing disease-related alterations in neural dynamics and motivate their validation in larger, independent cohorts and various other disease/cognitive states.

References

Braak, H., & Braak, E. (1991). Neuropathological staging of Alzheimer-related changes. Acta Neuropathologica, 82(4), 239–259. https://doi.org/10.1007/BF00308809

Debnath, A., Venot, T., Corsi, M.-C., & Verma, P. (2025). Neural mechanisms of training in brain-computer interface: A biophysical modeling approach. Preprint at bioRxiv. https://doi.org/10.1101/2025.06.21.660834

Donoghue, T. (2025). A systematic review of aperiodic neural activity in clinical investigations. European Journal of Neuroscience, 62(7), e70255. https://doi.org/10.1111/ejn.70255

Dubois, B., Villain, N., Schneider, L., et al. (2024). Alzheimer disease as a clinical-biological construct—An international working group recommendation. JAMA Neurology, 81(12), 1304–1311. https://doi.org/10.1001/jamaneurol.2024.3770

Hansen, P. C., & O'Leary, D. P. (1993). The use of the L-curve in the regularization of discrete ill-posed problems. *SIAM Journal on Scientific Computing, 14*(6), 1487–1503. https://doi.org/10.1137/0914086

He, B. J. (2014). Scale-free brain activity: Past, present, and future. Trends in Cognitive Sciences, 18(9), 480–487. https://doi.org/10.1016/j.tics.2014.04.003

He, B. J., Zempel, J. M., Snyder, A. Z., & Raichle, M. E. (2010). The temporal structures and functional significance of scale-free brain activity. Neuron, 66(3), 353–369. https://doi.org/10.1016/j.neuron.2010.04.020

Nedergaard, M., & Goldman, S. A. (2020). Glymphatic failure as a final common pathway to dementia. Science, 370(6512), 50–56. https://doi.org/10.1126/science.abb8739

Raj, A., Cai, C., Xie, X., et al. (2020). Spectral graph theory of brain oscillations. Human Brain Mapping, 41(11), 2980–2998. https://doi.org/10.1002/hbm.24991

Ranasinghe, K. G., Kudo, K., Syed, F., et al. (2025). Distinct manifestations of excitatory-inhibitory imbalance associated with amyloid-β and tau in patients with Alzheimer's disease. Nature Communications, 16, 7957. https://doi.org/10.1038/s41467-025-62798-4

Ranasinghe, K. G., Verma, P., Cai, C., et al. (2022). Altered excitatory and inhibitory neuronal subpopulation parameters are distinctly associated with tau and amyloid in Alzheimer's disease. eLife, 11, e77850. https://doi.org/10.7554/eLife.77850

Uhlhaas, P. J., & Singer, W. (2006). Neural synchrony in brain disorders: Relevance for cognitive dysfunctions and pathophysiology. Neuron, 52(1), 155–168. https://doi.org/10.1016/j.neuron.2006.09.020

van Blooijs, D., van den Boom, M. A., van der Aar, J. F., et al. (2023). Developmental trajectory of transmission speed in the human brain. *Nature Neuroscience, 26*(4), 537–541. https://doi.org/10.1038/s41593-023-01272-0

Verma, P., Nagarajan, S., & Raj, A. (2022). Spectral graph theory of brain oscillations—Revisited and improved. NeuroImage, 249, 118919. https://doi.org/10.1016/j.neuroimage.2022.118919

Verma, P., Nagarajan, S., & Raj, A. (2023). Stability and dynamics of a spectral graph model of brain oscillations. *Network Neuroscience, 7*(1), 48–72. https://doi.org/10.1162/netn_a_00263

Verma, P., Ranasinghe, K., Prasad, J., et al. (2024). Impaired long-range excitatory time scale predicts abnormal neural oscillations and cognitive deficits in Alzheimer's disease. Alzheimer's Research & Therapy, 16(1), 62. https://doi.org/10.1186/s13195-024-01426-7

Publishing Agreement

It is the policy of the University to encourage open access and broad distribution of all theses, dissertations, and manuscripts. The Graduate Division will facilitate the distribution of UCSF theses, dissertations, and manuscripts to the UCSF Library for open access and distribution. UCSF will make such theses, dissertations, and manuscripts accessible to the public and will take reasonable steps to preserve these works in perpetuity.

I hereby grant the non-exclusive, perpetual right to The Regents of the University of California to reproduce, publicly display, distribute, preserve, and publish copies of my thesis, dissertation, or manuscript in any form or media, now existing or later derived, including access online for teaching, research, and public service purposes.

Signed by:
Apurba Debnath
A13D50A9C4624B2...
Author Signature

08/24/2026
Date